光造形3Dフードプリンティングのフードインクの物理特性と応用に関する研究

Doctoral Dissertation

STUDY ON PHYSICAL PROPERTIES OF FOOD INKS AND THEIR APPLICATION IN STEREOLITHOGRAPHY 3D FOOD PRINTING

Graduate School of Marine Science and Technology
Tokyo University of Marine Science and Technology
Doctoral Course of Applied Marine Biosciences

RYO KOKI

Doctoral Dissertation

STUDY ON PHYSICAL PROPERTIES OF FOOD INKS AND THEIR APPLICATION IN STEREOLITHOGRAPHY 3D FOOD PRINTING

Graduate School of Marine Science and Technology
Tokyo University of Marine Science and Technology
Doctoral Course of Applied Marine Biosciences

RYO KOKI

Table of contents

1. General Introduction

1.1. Introduction and Objective

Three-dimensional (3D) food printing is an emerging technology which has the potential to create customized foods with targeted shapes, textures, and nutritional profiles through computer-aided design [1-3]. This technology is currently being studied for the development of high-functional foods in which the texture and taste can be freely adjusted to various requirements, such as easy-to-swallow foods for the elderly people. In addition, 3D food printing technology has recently been used in research for the development of meat analogs made from biopolymers, soybeans, and insects [4,5].

Four techniques of 3D food printing are available extrusion-based printing, inkjet printing, stereolithography printing, and binder jetting [6]. Currently, extrusion-based printing and stereolithography printing are generally studied by many research groups.

Stereolithography 3D food printing is a technology to create 3D food products by mixing vegetable and livestock powders and starches with water to prepare food ink, and then to heat the surface with laser irradiation to solidify the food inks through starch gelatinization. Then, this process is repeated to stack the solidified food ink layer by layer to make 3D printed foods [7,8]. This technology enables localized heating of food inks

with micron-order precision by laser irradiation, allowing for the manufacturing of 3D food products with complex shapes with formativeness, which is more advantageous over conventional extrusion 3D food printing. Several research have focused on the application of Stereolithography 3D food printing [7-13]. J. Bultinger et al. investigated in detail the differences in the heating behavior of wheat starch paste cooked with near-infrared (λ = 980 nm), mid-infrared (λ = 10.6 μm), and blue (λ = 445 nm) lasers. They showed that the gelatinized area in the starch paste heated by a 445 nm laser became largest compared to the paste heated by other lasers, suggesting that laser heating with a 445 nm laser is an effective cooking method for wheat paste, moreover, a combination of these different wavelengths can more efficiently heat wheat paste [11-13]. Despite these pioneering works, at the present time, there are several challenges hindering the industrial application of this technology. For instance, the preparation of food inks is difficult due to the low water uptake of powders made from food ingredients and furthermore, K.Rados et al, indicated that food inks prepared from powders with lower water uptake capacity exhibited reduced printability of 3D printed food [9]. Therefore, the water uptake behavior of food powders, which is the fundamental basis of these issues, needs to be elucidated. Additionally, the gelatinization behavior of starch in food inks after laser heating, which is intrinsically related to the formativeness of 3D printed food as well as

its texture and sensory properties remains unclear and needs to be clarified. Therefore, the aim of this study is to elucidate the water uptake behavior of food powders and the gelatinization behavior of starch by localized heating using laser irradiation from the perspective of food physical properties to realize the industrial application of stereolithography 3D food printing.

1.2. References

[1]. Le-Bail, Alain, Bianca Chieregato Maniglia, and Patricia Le-Bail. "Recent Advances and Future Perspective in Additive Manufacturing of Foods Based on 3d Printing." *Current Opinion in Food Science* 35 (2020): 54-64.

[2]. Mantihal, Sylvester, Rovina Kobun, and Boon-Beng Lee. "3d Food Printing of as the New Way of Preparing Food: A Review." *International Journal of Gastronomy and Food Science* 22 (2020): 100260.

[3]. Ling, Kenji C. L., Andrew Z. H. Yee, Chen Huei Leo, and Chee Kai Chua. "Understanding 3d Food Printing Technology: An Affordance Approach." *Materials Today: Proceedings* 70 (2022): 622-26.

[4]. Zhang, W., Y. Jia, C. Guo, S. Devahastin, X. Hu, and J. Yi. "Effect of Compositions and Physical Properties on 3d Printability of Gels from Selected Commercial Edible Insects: Role of Protein and Chitin." *Food Chem* 433 (Feb 1 2024): 137349.

[5]. Wen, Yaxin, Chhychhy Chao, Quang Tuan Che, Hyun Woo Kim, and Hyun Jin Park. "Development of Plant-Based Meat Analogs Using 3d Printing: Status and Opportunities." *Trends in Food Science & Technology* 132 (2023): 76-92.

[6]. Fernanda C. Godoi, Bhesh R. Bhandari, Sangeeta Prakash, Min Zhang, Fundamentals of 3D food printing and applications, Academic press, 2018

[7]. Jonkers, N., J. A. W. van Dommelen, and M. G. D. Geers. "An Anisotropic Elasto-Viscoplastic-Damage Model for Selective Laser Sintered Food." *Engineering Fracture Mechanics* 266 (2022). https://doi.org/10.1016/j.engfracmech.2022.108368.

[8]. Shahbazi, Mahdiyar, Henry Jäger, and Rammile Ettelaie. "Kinetic Evaluation of the Starch Molecular Behavior under Extrusion-Based or Laser Powder Bed Fusion 3d Printing Systems: A Systematic Structural and Biological Comparison." *Additive Manufacturing* 57

[9]. Blutinger J., Meijers Y., Hod L.. Selective laser broiling of Atlantic salmon. *Food Research International* , 120, 196-208 (2019) https://doi.org/10.1016/j.foodres.2019.02.043

[10]. J. Blutinger, A. Tsai, E. Storvick, G. Seymour, E. Liu, N. Samarelli, S. Karthik, Y. Meijers, H. Lipson. Precision cooking for printed foods via multiwavelength lasers. *npj Science of Food,* 5(24) 2021. http://creativecommons.org/licenses/by/4.0/.

[11]. J Blutinger, Y Meijers, PY Chen, C Zheng, E Grinspun, H Lipson. Characterization of dough baked via blue laser. *Journal of Food Engineering,* 232, 2018. https://doi.org/10.1016/j.jfoodeng.2018.03.022

[12]. J Blutinger, Y Meijers, PY Chen, C Zheng, E Grinspun, H Lipson. Characterization of CO2 laser browning of dough. *Innovative Food Science & Emerging Technologies* 52, 145-157, 2019, https://doi.org/10.1016/j.ifset.2018.11.013

[13]. PY Chen, J Blutinger, Y Meijers, C Zheng, E Grinspun, H Lipson. Visual modeling of laser-induced dough browning, *Journal of Food Engineering*, 243, 9-21, 2019. https://doi.org/10.1016/j.jfoodeng.2018.08.022

2. Background and basis of measurement

2.1. Starch gelatinization

Starch is a carbohydrate derived from plants and especially from crops in huge amounts. It includes amylose and amylopectin, which consists of α-1,4- and α-1,6-linked glucose units [1]. Starch granules are composed of amorphous and crystalline domains. The crystal structure is formed by the aggregation of amylopectin, which has a double helical structure, through hydrogen bonds [2]. There are three types of crystalline structure types in starch granules: type A, B, and C. The A-type, which is found in cereal starches, is characterized by monoclinic unit cells with 8 water molecules per unit cell and a greater proportion of short amylopectin chains. The B-type are found in tuber starches and consist of an open hexagonal unit cell with 36 water molecules and a greater proportion of long amylopectin chains. The C-type is a mixture of A- and B- types and is found in pulse starch [2].

The processing of starch-based foods such as rice, noodles, and bread, involves the gelatinization of starch, which occurs when starch is heated above about 60°C in the presence of water [3]. During gelatinization, the amorphous regions in the starch granules hydrate and swell, whereas the crystalline regions gradually melt with the proceeding hydration [4,5]. These processes largely affect textural and nutritional properties of

starch-based foods. On the other hand, the viscosity of the starch increases, and the destruction of the crystalline regions also imparts the starch higher sensitivity to enzymatic action, which improves its digestibility. For the stereolithography 3D food printing, the high viscosity of gelatinized starch is utilized to adhere each heated and solidified layers to form the designed food products [6]. Therefore, it is very important to study starch gelatinization for controlling quality of starch-based foods.

Various tools have been utilized to study the process of starch gelatinization, including the polarized microscope, small angle X-ray scattering (SAXS), X-ray diffraction (XRD), differential scanning calorimetry (DSC), scanning electric microscope (SEM), and rapid viscos analyzer (RVA) [6]. In particular, polarized microscope is commonly used to investigate the starch gelatinization by observing the starch crystal [4]. Moreover, SEM is a basic imaging technique for morphological analysis of starch granules [4]. Therefore, in this study, gelatinization of starch was investigated using polarized microscopy and SEM.

2.2. Magnetic Resonance Imaging (MRI) and T_2 relaxation time

Magnetic Resonance Imaging (MRI) is a technique which visualizes the spatial distribution of signal intensity, relaxation time, diffusion coefficient, and chemical shift obtained by nuclear magnetic resonance (NMR). It is widely used especially for

diagnostic imaging. This technology has great potential for non-invasive evaluation of food products, and its application is expected to be developed further [7].

Spin–spin relaxation time (T_2) of water protons can provide information about water mobility [8]. T_2 relaxation is used to measure the rate of relaxation in the transverse plane (x-y plane). It does exchange energy between spins, via a flip-flop type mechanism. The process causes a loss phase coherence between spins. T_2 relaxation time indicates the time it takes for that coherence to recover to equilibrium. The Carr-Purcell-Meiboom-Gill (CPMG) pulse sequence is widely used for measuring T_2 value, is given by

$$I(t) = I_0 \exp\left[-\left(\frac{t}{T_2}\right)\right]$$

where $I(t)$ is the signal intensity at echo time (t) and I_0 is initial signal intensity. T_2 relaxation time can be measured from the signal intensity indicated by T_2 weighted images taken with several different echo times and visualized by MRI.

There are several studies evaluating changes in water distribution during the noodle boiling process [9], salinity penetration process into fish meat [10], and the water absorption process of rice [11] from T_2 measurements by MRI. Additionally, measurements of water proton T_2 also provide information about starch-water interactions and the mobility of polysaccharide chains through chemical exchange between water protons and the exchangeable protons of polysaccharides [12]. Therefore, this method can

be used to visualize the spatial distribution of gelatinization state in the starch by MRI.

2.2. References

1). Junejo S. A., B. M. Flanagan, B. Zhang, and S. Dhital. "Starch Structure and Nutritional Functionality - Past Revelations and Future Prospects." *Carbohydr Polym* 277 (Feb 1 2022): 118837. https://doi.org/10.1016/j.carbpol.2021.118837.

2). Dongling Q, Binjia Z, Jing H, Fengwei X, David W, Fatang J, Siming Z, Jie Z. "Hydration-induced crystalline transformation of starch polymer under ambient conditions" *Int. J. Biol. Macromol.*103: 152-157. https://doi.org/10.1016/j.ijbiomac.2017.05.008.

3). Liu Hongsheng, Long Yu, Katherine Dean, George Simon, Eustathios Petinakis, and Ling Chen. "Starch Gelatinization under Pressure Studied by High Pressure Dsc." *Carbohydrate Polymers* 75, no. 3 (2009): 395-400. https://doi.org/10.1016/j.carbpol.2008.07.034.

4). Su Jinhan, Shuqi He, Suzhen Lei, Keqian Huang, Chuannan Li, Yi Zhang, and Hongliang Zeng. "Interaction Force between Laminaria and Different Crystal Starches Describes the Gelatinization Properties." *Food Hydrocolloids* 147 (2024). https://doi.org/10.1016/j.foodhyd.2023.109380.

5). Chi C., Y. Yang, S. Li, X. Shen, M. Wang, Y. Zhang, X. Zheng, and L. Weng. "Starch Intrinsic Crystals Affected the Changes of Starch Structures and Digestibility During Microwave Heat-Moisture Treatment." *Int J Biol Macromol* 240 (Jun 15 2023): 124297. https://doi.org/10.1016/j.ijbiomac.2023.124297.

6). Chi Chengdeng, Yiqing Zou, Xuemei Peng, Ying Yang, Bilian Chen, Yongjin He, Hongwei Wang, and Longmei Weng. "Measurement of Starch Gelatinization Using a Spectrophotometer." *Food Hydrocolloids* 144 (2023). https://doi.org/10.1016/j.foodhyd.2023.108956.

7). Kirtil Emrah, Sevil Cikrikci, Michael J. McCarthy, and Mecit Halil Oztop. "Recent Advances in Time Domain Nmr & Mri Sensors and Their Food Applications." *Current Opinion in Food Science* 17 (2017): 9-15. https://doi.org/10.1016/j.cofs.2017.07.005.

8). Sekiyama Yasuyo, Akemi K. Horigane, Hiroshi Ono, Kentaro Irie, Tatsurou Maeda, and Mitsuru Yoshida. "T2 Distribution of Boiled Dry Spaghetti Measured by Mri

and Its Internal Structure Observed by Fluorescence Microscopy." *Food Research International* 48, no. 2 (2012): 374-79. https://doi.org/10.1016/j.foodres.2012.05.019.

9). Fukuoka Mika, Mariko Oono, and Noboru Saka. "Magnetic Resonance Imaging and Microscopic Evaluation of the Effect of Flow on Water Migration During Noodle Cooking." *Journal of Agricultural Science and Food Technology* 4, no. 6 (2018): 120-29. http://pearlresearchjournals.org/journals/jasft/index.html.

10). Geonzon Lester C., Hannah A. Yuson, Kigen Takahashi, and Shingo Matsukawa. "Study on Salinity Penetration Process into Fish Meat by Simulation and Mri." *Fisheries Science* 87, no. 4 (2021): 609-17. https://doi.org/10.1007/s12562-021-01525-6.

11). Tomita Haruo, Mika Fukuoka, Toshikazu Takemori, and Noboru Sakai. "Development of the Visualization and Quantification Method of the Rice Soaking Process by Using the Digital Microscope." *Journal of Food Engineering* 243 (2019): 33-38. https://doi.org/10.1016/j.jfoodeng.2018.08.034.

12). Zhang Qiujin, Shingo Matsukawa, and Tokuko Watanabe. "Theoretical Analysis of Water 1h T2 Based on Chemical Exchange and Polysaccharide Mobility During Gelation." *Food Hydrocolloids* 18, no. 3 (2004): 441-49. https://doi.org/10.1016/j.foodhyd.2003.08.002.

3. Water uptake by freeze-dried potato and soybean powders: experiments and simulations

Abbreviations

r_0 capillary radius at the front of water uptake

ΔP_{cap} capillary pressure

θ contact angle between water and powder

ρ density of water

S_{eq} equilibrium value of S

g gravity acceleration

k kinetic coefficient

$\Delta p_{los}(i,j)$ pressure loss by water flow at the h_j

ΔP_{los} pressure loss of water

ρ_p powdered granule bulk density

R_p radius of powdered granule

r radius of the capillary

γ surface tension of water

Δt short time interval

i time interval index

v_i velocity of the water flow during $t = i\Delta t$

η viscosity of the liquid

t_{wet} wetting time

H_{p} water uptake height

h water uptake height in the capillary

W_{ex} water uptake weight

h_{∞} water uptake height at infinite time

W_{cal} water uptake weight calculated from water uptake height

h_{j} water heigh increment during jth interval

S $\frac{\eta}{r^2}$

3.1. Introduction

Powder technology is important to produce food powders that can be easily used in food products, such as tea, soup, and meat powders (Chen and Li 2009). Potato and soybean powders enjoy the greatest popularity and have been widely utilized in the food industry as beverage powders and in the production of health care products (Andrade et al. 2016; Petronia et al. 2012).

Freeze drying a low temperature drying process that utilizing sublimation, is a widespread technology in the food industry for preventing thermal degradation of valuable food nutrients, such as vitamins and colorants, and for maintaining original flavors (Karwacka et al. 2022; Lyu et al. 2022; Różyło 2020). The food powders obtained by freeze drying can uptake water rapidly to reproduce their original color and taste. For this reason, freeze drying is extensively utilized to produce food powders. Rapid water uptake, however, is not always desired (Wei et al. 2022). For instance, freeze-dried powders easily uptake moisture from the atmosphere during transport and storage (Mehra et al. 2022), not only causing observable changes in appearance and sensory attributes, but also leading to bacterial growth and powder aggregation (Fitzpatrick et al. 2017; Granados and Kawai 2021).

The water uptake process is initiated by wetting, hydration and swelling of the powders,

followed by powder dissolution, which is accompanied by an increase in viscosity. Capillary action experiments are widely used to evaluate the water uptake of food powders, such as polysaccharides (See et al. 2023; Wangler and Kohlus 2017, 2018; Wangler et al. 2019), milk proteins (McSweeney et al. 2021, Opaliński et al. 2016), wheat flour (Fu et al. 2017) and apple powder (Wei et al. 2022). Wangler and Kohlus (2017) adopted a mathematical model based on the Lucas–Washburn's equation to simulate the water uptake of food powders. According to their model, powder granules are represented as numerous capillaries that absorb water by capillary action. Wangler and Kohlus (2017) considered the change in capillary radius due to powder swelling and the change in solution viscosity following powder dissolution. This model was able to qualitatively simulate water uptake and evaluate the effects of powder swelling and viscosity changes. Fries and Dreyer (2008) proposed a mathematical model of the capillary rise of water that includes the effect of gravity. This model, however, does not consider the difference in powder swelling and viscosity due to variable water uptake rates between powders.

In this study, we elucidated the water uptake behavior of freeze-dried potato and soybean powders through capillary action and magnetic imaging resonance (MRI) experiments, the latter being a non-invasive tool to study water distribution in food matrices (Hall et al. 1998; As and Duynhoven 2013). In addition, a numerical simulation based on a

modified version of Fries and Dreyer's (2008) mathematical model was performed to clarify the effects of powder swelling and viscosity.

3.2. Materials and methods

3.2.1. Materials

Potato powder was purchased from NICHIGA Co., Ltd., (Japan). Soybean powder was purchased from Mitake Food Mfg. Co., Ltd., (Japan). According to the suppliers, the potato powder is 80.8% carbohydrates, 7.8% protein, 1.2% fat and 0.22% sodium; while the soybean powder is 39.9% protein, 28.8% carbohydrates and 22.2% fat. These compositions are similar to those reported in other works (Osthoff et al., 2010; Petronia et al., 2012; Sablani and Mujumdar, 2006; Yang et al., 2022).

The potato and soybean powders were dispersed at a concentration of 30% in deionized water at room temperature to obtain homogeneous powder pastes. The potato paste was molded with a thickness and width of 1 mm using a noodle-making machine (ATLAS 150, Italy) capable of forming the dough into various shapes. Molds were frozen at -30 °C for 12 h and then lyophilized at -75 °C for 24 h in a freeze dryer (GLD-136C, ULVAC, Japan). The soybean paste was filled into a sandwich-like iron plate with a 1 mm space and then was frozen at -30 °C for 12 h, after which the frozen soybean paste was cut to 1 mm thick slices and immediately freeze dried at -75 °C for 24 h. The lyophilized

potato and soybean pastes were grinding and filtered, respectively, to obtain granules of 1–3 mm in size.

3.2.2. Characterization of freeze-dried potato and soybean powder granules

Moisture content of the freeze-dried potato and soybean powdered granules was measured as follows: The samples of powdered granules were each placed in a drying oven (DS400; YAMATO scientific Co., Ltd, Japan) at 105°C for 5 hours to dry, and the water content was determined from the ratio of the weights of the samples before and after drying. The moisture contents for both of potato and soybean powdered granules were approximately 1.1%.

Particle size distribution was measured as follows: Forty samples of powdered granules were randomly selected and photographed with a camera. The area of the powdered granules was measured with Image J software (NIH, version 1.52), and the particle diameter was approximated as the diameter of a circle of the same surface area. The diameter of potato and soybean powdered granules ranged from 1.5 to 3 mm.

The contact angle between the powder and deionized water was determined by the sessile drop method at 25°C (Lazghab et al., 2005). The potato and soybean powders were separately dispersed in deionized water at room temperature under continuous stirring to obtain a homogeneous (50%) paste. Paste (10 mL) was spread on an iron plate to obtain

a smooth sheet. The sheet was dried at room temperature (25°C) with a drying time of 48 hours. The contact angle between the sheet and water was measured by dropping 50 μL of deionized water onto the sheet from 1 cm above the plate and the angle between water droplet and sheet was measured by protractor. The shape of the water droplet was recorded using a digital microscope (nano. capture PRO, SIGHTRON JAPAN, Japan).

3.2.3. Water uptake experiments

Water uptake by potato and soybean powdered granules was evaluated by capillary action experiments (Wangler and Kohlus 2017) carried out in an incubator at 25 °C using the setup shown in Fig. 1. The freeze-dried powdered granules were filled into a plastic tube of 1 cm diameter fitted with a tissue paper at the bottom. Water could be absorbed through the tissue paper. Water uptake weight (W_{ex}) was measured with an electronic scale. The water uptake height was monitored with a digital microscope (nano. capture PRO, SIGHTRON JAPAN, Japan). The water uptake weight calculated from water uptake height (W_{cal}) can be expressed as follows:

$$W_{\mathrm{cal}} = H_{\mathrm{p}}\pi {R_{\mathrm{p}}}^2\rho - H_{\mathrm{p}}\pi {R_{\mathrm{p}}}^2\rho_{\mathrm{p}}$$

$$= \pi {R_p}^2 H_p(\rho - \rho_{\mathrm{p}}) \quad (1)$$

where H_{p} is the water uptake height within the powdered granule bulk, R_{p} is radius of the powdered granule bulk, ρ is the density of water, ρ_{p} the powdered granule bulk

density, determined experimentally as 229 kg/m^3. Each experiment was repeated three times.

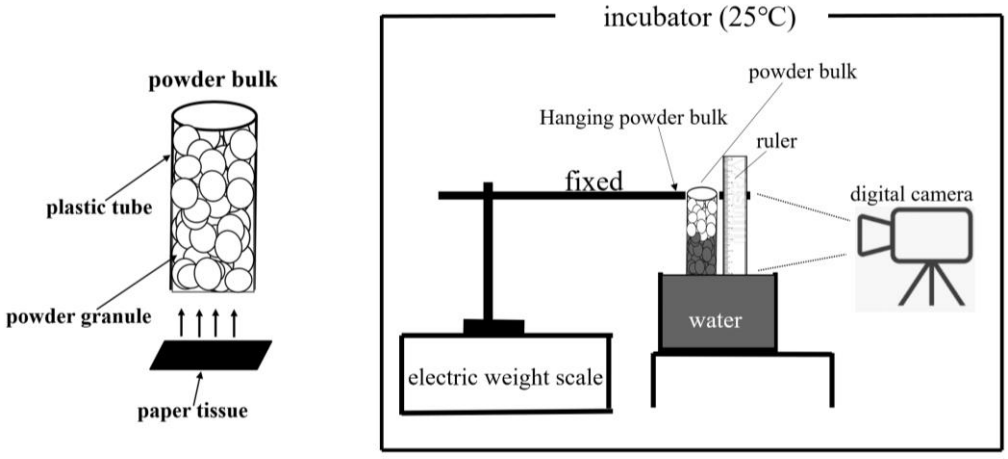

Fig. 1. Schematic diagram of the experimental setup.

3.2.4. MRI

Water uptake by potato and soybean powdered granules was studied by MRI (AVANCE400WB, Bruker BioSpin Co. Ltd., Germany). Freeze-dried powdered granules which filled into a plastic tube of 1 cm diameter were placed in a plastic container with a 3 cm diameter together with 5 mL of deionized water. The container was immediately placed in an MRI probe and studied using a FLASH sequence, which is a high-speed NMR imaging technique using flip angles well below 90°. Each MRI measurement was performed 10 times, with repetition time = 3.4 ms, echo time = 1.4 ms, number of pixels = 128 × 128, slice thickness = 1 mm, scan number = 4.

3.2.5. Simulation of water uptake

Numerical simulations are expected to provide insights on the effects of powder swelling and solution viscosity on water uptake. Wangler and Kohlus (2017) performed a numerical simulation based on Washburn's model, where the solution viscosity was assumed to be homogeneous. In this model, the pores were assumed to be uniformly distributed in the powder and can be described by numerous capillaries. They found that the swelling of powder and the increase of solution viscosity reduced the rate of water uptake. Fries and Dreyer developed a mathematical model of the capillary rise of water in capillary that considered the effect of gravity (Fries and Dreyer 2008). The capillary pressure ΔP_{cap} $(\mathrm{N/m^2})$ was expressed as the difference between the Laplace pressure and the pressure due to the weight of absorbed water:

$$\Delta P_{\mathrm{cap}} = \frac{2\gamma Cos\theta}{r_0} - \rho g h \tag{2}$$

where $\gamma(\mathrm{N/m^2})$, $\theta(^\circ)$ and r_0 (mm) represent the surface tension of water, the contact angle between water and powder, and the radius of the capillary at the front of water uptake, respectively; $\rho(\mathrm{kg/m^3})$, $g(\mathrm{m/s^2})$ and h (m) represent the density of water, gravity acceleration, and the water height in the capillary, respectively.

The pressure loss of water ΔP_{los} $(\mathrm{N/m^2})$ in the capillary due to laminar flow of water was expressed by the Hagen-Poiseuille's equation,

$$\Delta P_{los} = 8h\frac{\eta}{r^2}\frac{dh}{dt} \quad (3)$$

where $\eta(\ N/m^2.s)$ is the viscosity and r (mm) is the radius of the capillary, which can be interpreted as the pore size in powder. When a steady state is reached, $\Delta P_{cap} = \Delta P_{los}$, and eqs. (2)–(3) yield:

$$\frac{dh}{dt} = \frac{\rho g}{8h}\frac{r^2}{\eta}\left(\frac{2\gamma Cos\theta}{r_0\rho g} - h\right) \quad (4)$$

Eq. (4) can be solved with the initial condition of $h = 0$ at t=0, to give

$$h(t) = h_\infty(1 + W[-exp\ (-1 - \frac{\rho g}{8h_\infty}\frac{\eta}{r^2}t)]) \quad (5)$$

where W is the Lambert W function, defined as an inverse function of $f(x) = xexp\ [x]$, and h_∞ is the water uptake height at infinite time, equal to $2\gamma Cos\theta/r_0\rho g$.

In this study, numerical simulations based on a gravity-corrected Washburn-model (equation 5) were performed to study the effects of powdered granules swelling and viscosity changes using a lab made program by the Mathematica 12 (Wolfram, USA).

3.3. Results and discussion

3.3.1. Contact angle of potato and soybean powders

Contact angle is an important parameter for evaluating the wettability of powders with water (Oostveen et al. 2015). The contact angles of potato and soybean powders with water were 30 and 40°, respectively, as shown in Fig. 2. This result indicates that both powders possess limited wettability. In addition, potato powder exhibited a lower contact

angle, indicating it was more hydrophilic and wettable than soybean powder, which contains more fat.

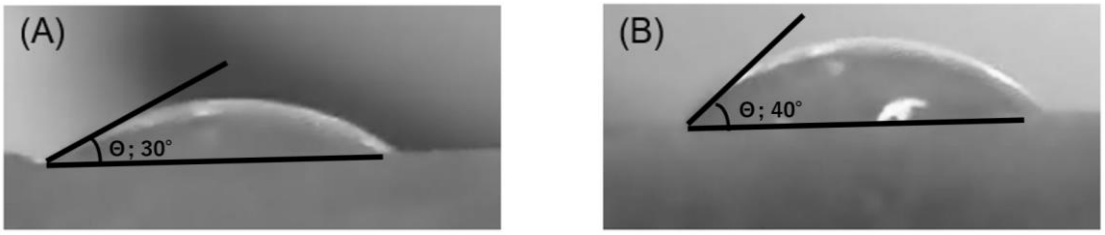

Fig. 2. Contact angle between water and (A) potato or (B) soybean powder

3.3.2. Water uptake experiments

The water uptake behavior of powdered granules was investigated by measuring their water uptake weight (W_{ex}) and the calculated weight (W_{cal}) from the experimental water uptake height followed by Eq. 1. Fig. 3 presents water uptake of freeze-dried potato and soybean powdered granules as a function of time. Red and blue lines indicate W_{cal} of potato and soybean powdered granules, respectively. Purple and green lines indicate W_{ex} of potato and soybean powdered granules, respectively.

For the potato powdered granules, W_{cal} rapidly increased in the initial 10 min, followed by a gradual and continuous increase. The driving force of water uptake is the constant capillary force in the porous internal structure of the powdered granules. As water is absorbed, the force due to gravity of water filling the porous structure increases, as reflected in W_{cal}. After 30 min, W_{cal} approached a plateau, with a water uptake weight of around 3.0 g.

For the soybean powdered granules, on the other hand, W_{cal} rapidly increased in the initial 2 min, followed by a gradual and continuous increase. W_{cal} approached a plateau with a water uptake weight of around 1.1 g after 30 min. These results indicate the higher water uptake capability of the potato powdered granules. The higher uptake can be ascribed to the powder composition, which also affected the contact angle. We note that the experimental results of water uptake weight (W_{ex}) of both granules showed the same behavior as the calculated water uptake weight (W_{cal}), respectively. However, W_{cal} was approximately 20% larger than W_{ex} shown in Fig. 3, suggesting the formation of air bubbles in the powdered granules.

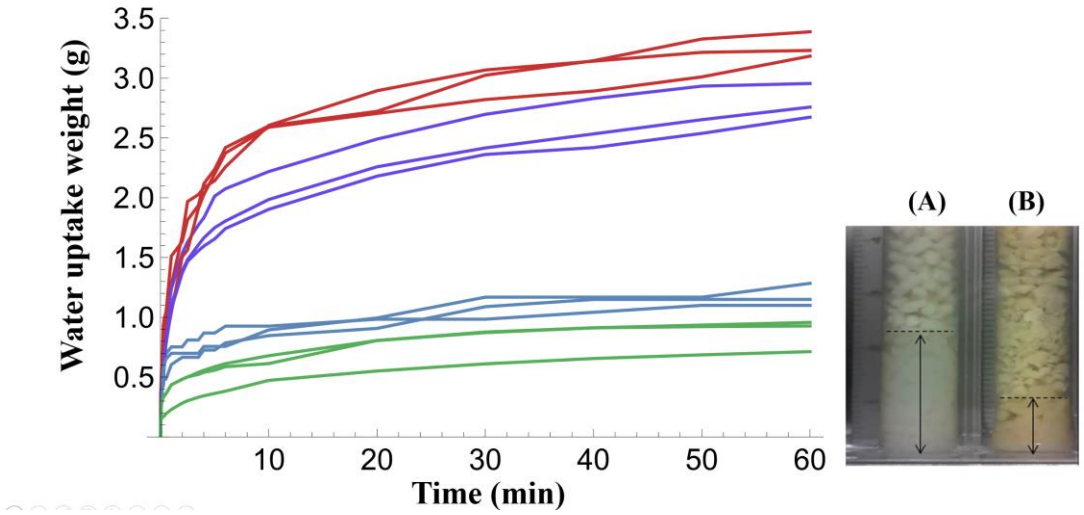

Fig. 3. Water uptake of freeze-dried potato and soybean powdered granules. Red and blue lines indicate values calculated from the water uptake height of potato and soybean powdered granules, respectively. Purple and green lines indicate experimental results of water uptake weight of potato and soybean powdered granules, respectively. Images were taken after 2 min of water uptake; (A) Potato and (B) soybean powders.

Images of potato and soybean powdered granules after 2 min of water uptake are presented as insets in Fig. 3. At 2 min of water uptake, the potato powdered granules exhibited considerable swelling, keeping their original shape. In contrast, soybean powdered granules dispersed in water quickly and the water channels collapsed, which slowed down further absorption of water. These results demonstrate that the difference in the water uptake comes from the differences in swelling and dispersing in water. Although powdered granule dissolution was not observed directly in these experiments, it certainly increased the solution viscosity for both granules, thus slowing down water uptake (Wangler and Kohlus 2017).

3.3.3. MRI measurements

MRI a is useful tool for studying the water distribution in food (As and

Duynhoven 2013). MRI experiments were performed to elucidate the water uptake of potato and soybean powdered granules as a function of time. Fig. 4 presents MRI images of swelling granules. Brighter areas indicate higher water contents. In the following, t indicates time from the beginning of the experiment. At t = 1.7 s, a black area was observed for potato granules, corresponding to gaps between granules. Images taken t = 3.4 and 5.1 s showed that these black areas disappeared, indicating water uptake into these intergranular gaps. At longer times, the total water content increased, both within and between granules. Water content increased monotonously up to t = 20.4 s, but gaps present at this stage remained the same up to t = 10 minutes. These gaps were probably attributed to air bubbles inside the powdered granule bulk. Formation of air bubbles can be expected, as the gaps between powdered granules are large and only weak capillary forces act within them. Formation of air bubbles can also account for W_{cal} being 20% larger than W_{ex}. Soybean powdered granules were more easily dispersed than potato powdered granules, and thus filled in the gaps and showed fewer and smaller air bubbles.

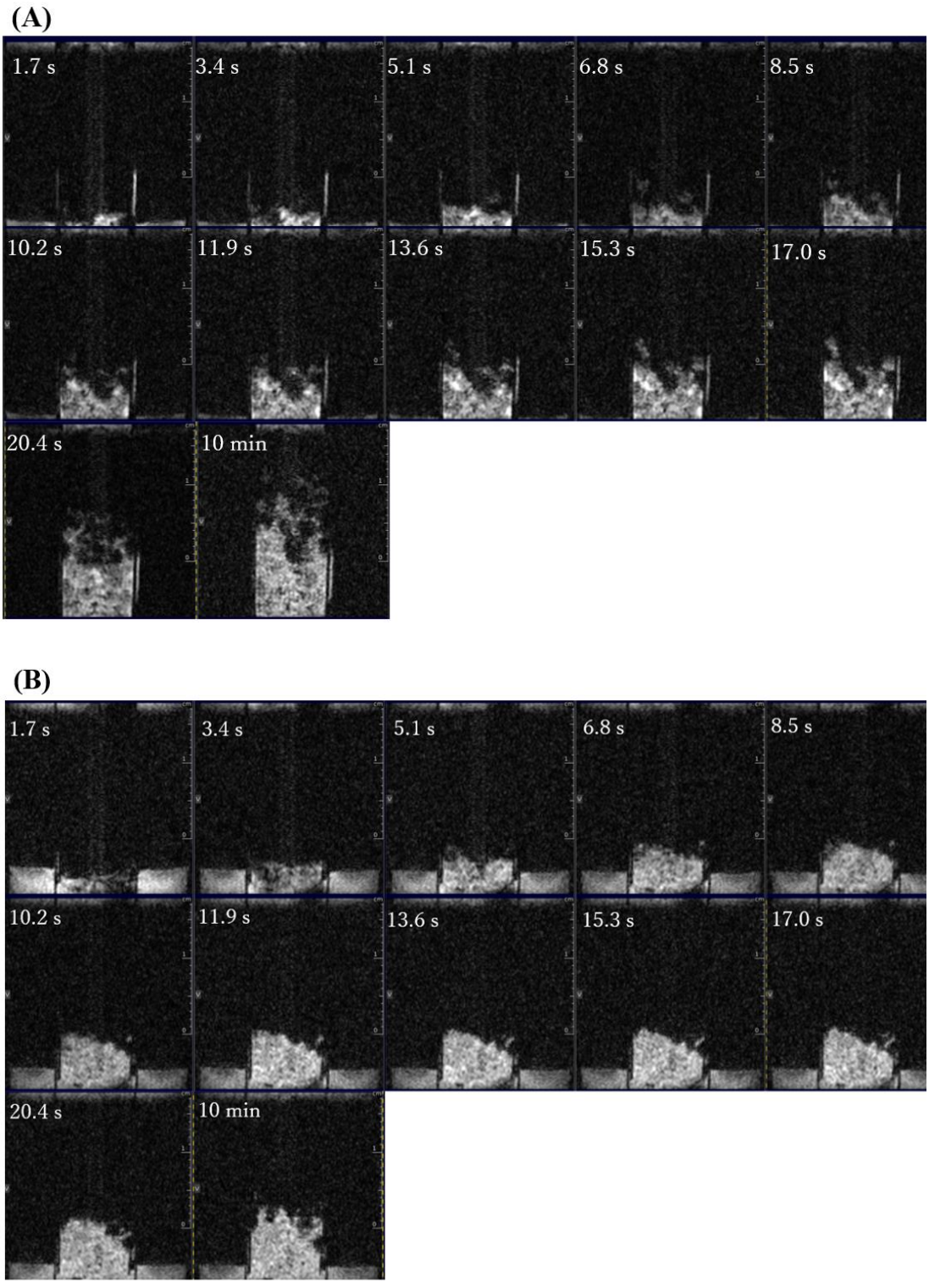

Fig. 4. MRI images of freeze-dried (A) potato and (B) soybean powdered granules at different water absorption times.

3.3.4. Numerical simulations

A numerical simulation that takes the viscosity changes into account was carried out to study their effects. According to our model, water uptake leads to changes in r and η as the granules swell and viscosity increases. It should be noted that the change of r and η can be expressed as $S = \eta/r^2$ in the Hagen Poiseuille equation (Eq. 3). For considering the effect of time-dependent r and η, we used the following first order differential equation as a simple model, where we considered that the swelling and viscosity increase rate is proportional to the difference between S and the degree of S at the equilibrium (S_{eq}). Then, the following equation holds:

$$\frac{dS}{dt_{\mathrm{wet}}} = k\left(S_{\mathrm{eq}} - S\right) \tag{6}$$

where, t_{wet} k, are the wetting time, and a kinetic coefficient, respectively. Under the condition of $S = S_0$ at $t_{\mathrm{wet}}=0$, Eq. (6) gives

$$S(t_{\mathrm{wet}}) = S_{\mathrm{eq}} - (S_{\mathrm{eq}} - S_0)exp\,[-k\,t_{\mathrm{wet}}] \tag{7}$$

To account for changes in S following wetting, we carried out a recursive calculation of the water height based on Eq.(4), which becomes the following equation by using $S(t_{\mathrm{wet}})$,

$$h(t) = h_{\infty}(1 + W[-exp\,(-1 - \frac{\rho g/S}{8h_{\infty}}\,t)]) \tag{8}$$

We considered a short time interval Δt where S is approximately constant. The total experiment time t is $i\Delta t$ and the water height increment during the jth interval is h_j. S

during the first-time interval (S_0) can be expressed using the initial values of r and η (r_0 and η_0) as $S_0 = \eta_0 / r_0^2$ to give the height of water uptake as:

$$h_1 = h_\infty (1 + W[-\exp(-1 - \frac{\rho g / S_0}{8 h_\infty} \Delta t)]) \quad (9)$$

As shown in Fig. 5(A), S in the wet granule changes according to Eq.(7) as follows:

$$S(i,j) = S_{\mathrm{eq}} - (S_{\mathrm{eq}} - S_0) \exp[-k(t - (i-j)\Delta t)] \quad (10)$$

Considering the change of $S(i, j)$, Δp_{los} becomes

$$\Delta p_{\mathrm{los}}(i,j) = 8 h_j S(i,j) v_{\mathrm{i}} \quad (11)$$

where v_{i} is the velocity of water flow at t = $i\Delta t$ and is constant across the wet powdered granule sample. The total pressure loss is then:

$$\Delta P_{los} = \sum_j^{i-1} \Delta p_{\mathrm{los}(i,j)} \quad (12)$$

which should be equal to ΔP_{cap} in Eq. (2), yielding

$$v_{(t=i\Delta t)} = \frac{2\gamma Cos\theta / r_0 - \rho g \sum_j^{i-1} h_{\mathrm{j}}}{\sum_j^{i-1} 8 S(i,j) h_{\mathrm{j}}} \quad (13)$$

Δh_{i} (the water height increment during Δt at t = iΔt) is calculated as follows (see Fig. 5(B))

$$\Delta h_{\mathrm{i}} = v_{(t=i\Delta t)} \Delta t \quad (14)$$

The Total water uptake height, $h(t)$ was calculated by recursively carrying out the calculation using equations Eqs. (10)–(14).

Fig. 5(C) shows numerical simulation results. A value of k = 0 corresponds to

constant capillary radii and solution viscosities. The water uptake height increased quickly at the beginning and gradually approached a plateau. For $k = 0.01$ and 0.1, a quick initial increase is observed, which slows down due to changes in r and η, indicating that increasing capillary radii and viscosities both delay water uptake. This result agrees with the experimental results shown in Fig. 3. Our model could therefore capture the effects of viscosity and pore radii of swelling powdered granules on water uptake.

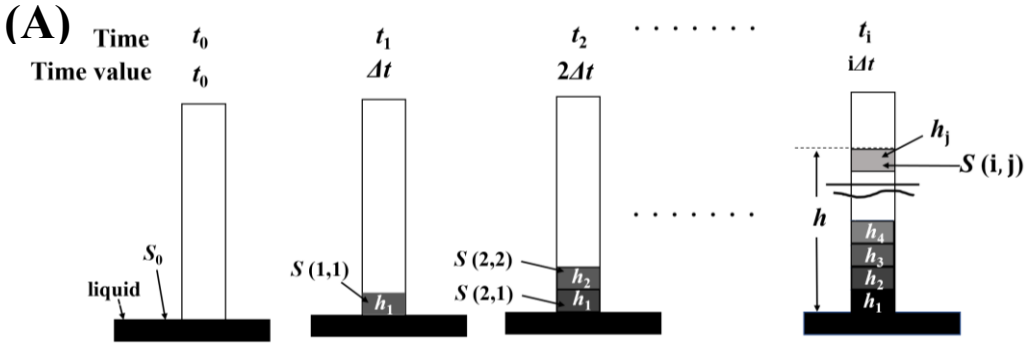

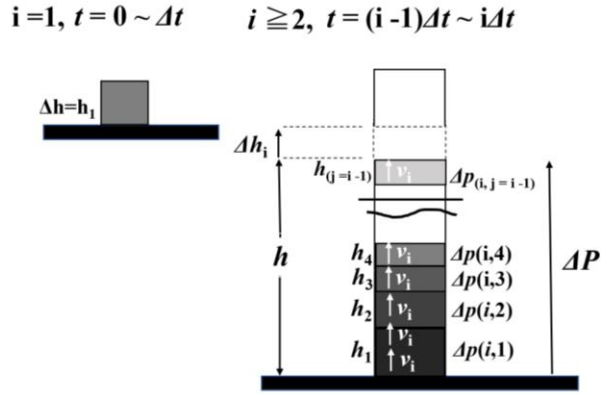

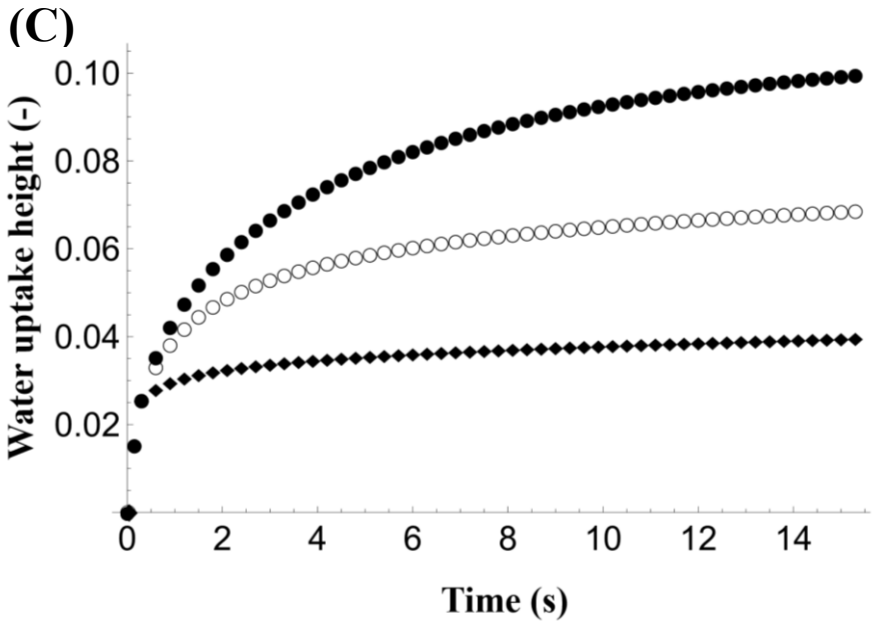

Fig. 5. Schematic illustration of the theoretical simulation. (A): Evolution of viscosity and capillary radius; (B): modeling water uptake height; (C): simulation results with k = 0 (●), k = 0.01 (○)and k = 0.1 (◆).

3.4. Conclusions

The water uptake of freeze-dried granules of potato and soybean powders was studied by capillary action and MRI experiments. Due to their different compositions, the potato and soybean powdered granules exhibited different wettability and swelling properties. These differences gave rise to different water uptake capacities. The potato powder contained less oil than the soybean powder, and thus absorbed more water. On the other hand, the qualitative features of the water uptake process were similar for the two powdered granules, with a high initial water uptake rate that gradually decreased. The difference between W_{cal} and W_{ex} suggested that presence of air bubbles affected water uptake. MRI measurements gave experimental evidence of air bubbles forming during water absorption. A numerical simulation model that accounts for powder swelling and solution viscosity was proposed. It was demonstrated that the increase in solution viscosity and pore size delayed caused the decrease in the rate of water uptake. The qualitative features captured by this simulation agree with the experimental results observed for the potato and soybean powdered granules.

3.5. References

Andrade JC, Mandarino JG, Kurozawa LE, Ida EI (2016) The effect of thermal treatment of whole soybean flour on the conversion of isoflavones and inactivation of trypsin

inhibitors. Food Chem 194: 1095-1101. https://doi.org/1010.1016/j.foodchem.2015.1008.1115.

As HV, Duynhoven J (2013). MRI of plants and foods. J Magnetic Resonance 229: 25-34. https://doi.org/10.1016/j.jmr.2012.1012.1019.

Chen XD, Li D. (2009) Food powder technology. J Food Eng 94(2): 129. https://doi.org/110.1016/j.jfoodeng.2009.1002.1027.

Fitzpatrick JJ, O'Connor J, Cudmore M, Dos S D. (2017) Caking behavior of food powder binary mixes containing sticky and non-sticky powders. J Food Eng 204: 73-79. https://doi.org/10.1016/j.jfoodeng.2017.1002.1021.

Fries N, Dreyer M. (2008) An analytic solution of capillary rise restrained by gravity. J Colloid and Interface Science 320: 259-263. https://doi.org/210.1016/j.jcis.2008.1001.1009.

Fu BX, Wang K, Dupuis B. (2017) Predicting water absorption of wheat flour using high shear-based GlutoPeak test. J Cereal Science 76: 116-121. https://doi.org/110.1016/j.jcs.2017.1005.1017.

Granados AEA, Kawai K. (2021) Effect of cellulose powder content on the water sorption, glass transition, mechanical relaxation, and caking of freeze-dried carbohydrate blend and food powders. Lwt 148: 111798. https://doi.org/111710.111016/j.lwt.112021.111798.

Hall LD, Evans SD, Nott KP (1998) Measurement of textural changes of food by MRI relaxometry. Magnetic Resonance Imaging 16: 485–492. https://doi.org/10.1016/S0730-725X(98)00116-7

Hellborg D., Bergenståhl B., Trägårdh C. (2012). The influence of powder properties on the imbibation rate. Colloids Surf. B. 93(1). 108-115. https://doi.org/10.1016/j.colsurfb.2011.12.023

Karwacka M, Ciurzyńska A, Galus S, Janowicz M (2022). Freeze-dried snacks obtained from frozen vegetable by-products and apple pomace – Selected properties, energy consumption and carbon footprint. Inn Food Science & Emerging Tec 77: 102949. https://doi.org/102910.101016/j.ifset.102022.102949.

Lazghab M, Saleh K, Pezron I, Guigon P, Komunjer L (2005). Wettability assessment of finely divided solids. Powder Tec 157: 79-91. https://doi.org/10.1016/j.powtec.2005.1005.1014.

Lyu Y, Bi J, Chen Q, Wu X, Gou M, Yang X (2022). Color enhancement mechanisms analysis of freeze-dried carrots treated by ultrasound-assisted osmosis (ascorbic acid-CaCl2) dehydration. Food Chem 381: 132255. https://doi.org/132210.131016/j.foodchem.132022.132255.

McSweeney DJ, Maidannyk V, O'Mahony JA, McCarthy NA (2021). Rehydration properties of regular and agglomerated milk protein concentrate powders produced using nitrogen gas injection prior to spray drying. J Food Eng 305:110597. https://doi.org/110510.111016/j.jfoodeng.112021.110597.

Mehra R, Kumar S, Singh R, Kumar N, Rathore D, Nayik GA, Alabdallah NM, Monteiro A, Guine RFF, Kumar H (2022). Biochemical, dielectric and surface characteristics of freeze-dried bovine colostrum whey powder. Food Chem X 15: 100364. https://doi.org/100310.101016/j.fochx.102022.100364.

Oostveen MLM, Meesters GMH, Ommen JRV (2015). Quantification of powder wetting by drop penetration time. Powder Technology 274: 62-66. https://doi.org/10.1016/j.powtec.2014.1009.1021.

Opaliński I, Chutkowski M, Hassanpour A (2016). Rheology of moist food powders as affected by moisture content. Powder Technology 294: 315-322. https://doi.org/310.1016/j.powtec.2016.1002.1049.

Osthoff G, Hugo A, Wyk P, Wit M. (2010). Characterization of a Spray-Dried Soymilk Powder and Changes Observed During Storage. Food Science and Technology International 16: 169-178. https://doi.org/110.1177/10820132093532.

Petronia C, Cacace D, Pascale SD, Rapacciuolo M, Fuggi A (2012). Organic vs. traditional potato powder. Food Chem 133: 1264-1273. https://doi.org/1210.1016/j.foodchem.2011.1208.1088.

Różyło R (2020). Recent trends in methods used to obtain natural food colorants by freeze-drying. Trends in Food Science & Technology 102: 39-50. https://doi.org/10.1016/j.tifs.2020.1006.1005.

Sablani SS, Mujumdar AS (2006). Drying of Potato, Sweet Potato, and Other Roots. Handbook of Industrial Drying, In Mujumdar A. S., eds, Chapter 27. Taylor & Francis Group, LLC. https://doi.org/10.1201/9781420017618

See XY, Dupas-Langlet M, Forny L, Meunier V, Zhou W (2023). Physical stability of co-freeze-dried powders made from NaCl and maltodextrins – Impact of NaCl on glass

transition temperature, water vapour sorption isotherm and water vapour sorption kinetics. Food Hydrocolloids 136: 108238. https://doi.org/108210.101016/j.foodhyd.102022.108238.

Wangler J, Kohlus R (2017). Dynamics of Capillary Wetting of Biopolymer Powders. Chemical Engineering & Technology 40: 1552–1560. https://doi.org/1510.1002/ceat.201600607.

Wangler J, Kohlus R (2018). Development and validation of methods to characterize rehydration behavior of food hydrocolloids. Food Hydrocolloids 82: 500-509. https://doi.org/510.1016/j.foodhyd.2018.1004.1018.

Wangler J, Teichmann H, Konstanz E, Kohlus R (2019). Experimental investigation and simulation of rehydration dynamics of biopolymer powders. Powder Technology 355: 461-473. https://doi.org/410.1016/j.powtec.2019.1007.1022.

Wei Y, Yang X, Jiang S, Liang H, Li B, Li J (2022). Anti-hygroscopic effect of wheat gluten on freeze-dried apple powder. Lwt 167: 113887. https://doi.org/113810.111016/j.lwt.112022.113887.

Yang L, Wang S, Zhang H, Du C, Li S, Yang J (2022). Effects of black soybean powder particle size on the characteristics of mixed powder and wheat flour dough. Lwt 167: 113834. https://doi.org/113810.111016/j.lwt.112022.113834.

4. Study on gelatinization of wheat starch paste by localized heating using laser irradiation and subsequent water migration

4.1. Introduction

Laser cooking is an emerging technique with a potential application in the food industry because it enables the highly localized cooking in micron-order precision with a rapid heat increasing [1-4], which has an outstanding benefit in 3D food printing [5-7]. When the surface of starch food inks are heated by a laser irradiation, starches will gelatinizes and then solidify quickly, to make layer-by-layer stacks of 3D printed foods[8]. Therefore, it is important to understand the gelatinization behavior and the water distribution in the starch pastes under laser heating because these behaviors are intrinsically related to the formativeness of 3D printed food and also food texture, and sensory properties. Currently, there are several studies that have revealed the potential use of starch pastes for laser cooking technology. [8-10]. However, the understanding for gelatinization behavior of starch granules under laser cooking is still lacking in fundamental aspects, e.g., the change of water distribution in the starch paste during gelatinization by laser heating. In the present study, the gelatinization behavior of a wheat paste under the radiation of a laser was studied, and the subsequent change in water distribution in wheat paste was revealed using magnetic resonance imaging (MRI). This work is expected to provide valuable information on the effect of laser heating on starch food materials.

4.2. Material and Methods

4.2.1 Sample preparation

Wheat flour was purchased from Nisshin Seifun Welna Inc. (Japan) and stored in desiccator at RH=0% for further use. The wheat flour comprises 76.6% carbohydrate, 7.7% protein, and 1.4% fat, without sodium salt. The green food dye was purchased from Kyoritsu Food Inc. (Japan), and composed of 88% dextrin, 4.8% tartrazine, and 3.6% brilliant blue FCF.

The wheat paste was prepared by mixing the wheat flour with distilled water at room temperature to achieve 50% concentration (*w/w*) under continuous stirring. The green dye was then added the wheat paste under homogeneous mixing to obtain 0.1% (w/w) of dye concentrations, respectively.

4.2.2 Laser heating

A 5 W (450 nm wavelength) blue diode laser (laser pecker2; Shenzhen Hingin Technology Co., Ltd, China) was used to heat the wheat paste in one direction following a 30-mm straight line under radiation by the laser at a scan speed of 13 mm/s. Meanwhile, the surface and cross-section of the wheat paste were photographed with a digital microscope (nano. capture PRO; SIGHTRON JAPAN, Japan).

An IR camera (InfReC; NIPPON AVIONICS Co., Ltd, Japan) was used to measure the temperature distribution of the surface of the wheat paste during laser heating. The temperature profile was calculated from the temperature of the pixels on the IR image using software (Avio

NS9500 InfReC Infrared analyzer; NIPPON AVIONICS Co., Ltd, Japan).

4.2.3 Optical and polarization microscope observation

The crystals of starch granules in the wheat paste-induced by laser heating were examined using a polarized microscope (BX50; Olympus, Japan). The sample was prepared by sandwiching the wheat paste between two cover glasses with a spacer of aluminum foil with thickness of around 12 μ m, and buried in a bulk wheat paste (Fig. 1), and scanned by the laser, followed by observing the cross-section of the paste by optical and polarized microscopy.

4.2.4 Scanning electron microscope (SEM) observation

The sample used in Section 4.2.3 was quickly frozen by soaking in liquid nitrogen and then freeze-dried to prepare samples for SEM observation. For the measurement, dried samples were deposited on a copper disc and coated with platinum palladium using an ion sputter (E-1030; HITACH, Japan). The sample was examined using FE-SEM (S-4000; HITACH, Japan) at 10 kV accelerating voltage.

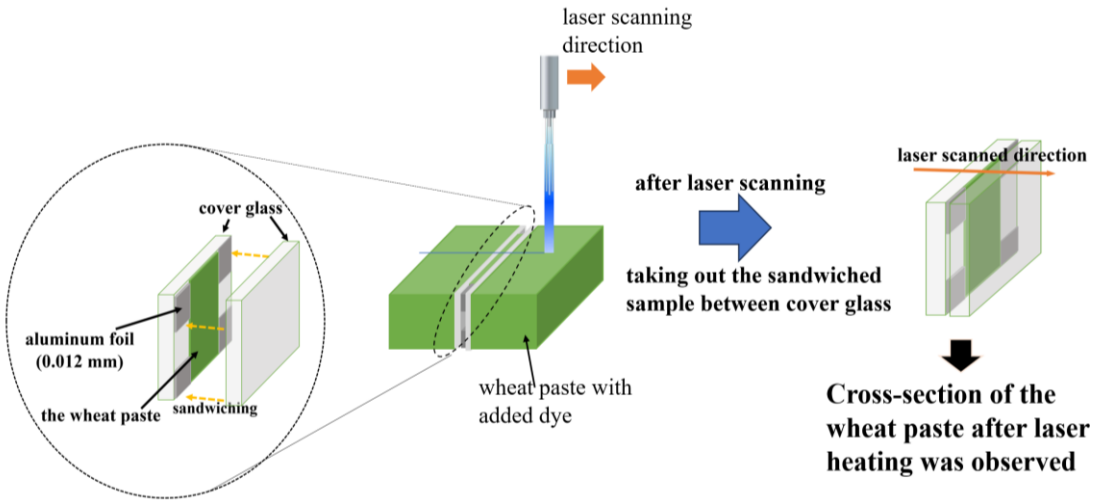

Fig. 1 Schematic diagram of the experimental setup.

4.2.5 MRI

Water ^{1}H T_2 of wheat paste after laser heating was measured by high-resolution MRI (AVANCE400WB; Bruker, Germany) of 9.4 T equipped with a ^{1}H rf coil with a diameter of 20 mm. A semi-cylindrical tube with a diameter of 4.0 mm was filled with wheat paste with 0.1% (w/w) dye. The laser was then scanned in one direction and its cross-section was visualized as T_2 weighted image. MRI measurements were performed with repetition time = 1 s, echo time = 9.4 ms, number of pixels = 256 × 256, slice thickness = 1 mm, and scan number = 4. A 40% concentration of sugar solution was used as a reference.

4.2.6 Water content of model paste sheet

To confirm the result of MRI measurement, the water content of locally heated and unheated regions of the wheat paste was measured, respectively. Wheat paste sheet containing 50%(*w/w*) water content was prepared with 1 mm thickness using a spacer and placed on a cooling plate kept at 0°C. Then, the paste sheet was heated by placing an iron plate at 200°C on top of it for gelatinizing the starch. The gelatinized and non-gelatinized regions of the wheat paste were each placed in a drying oven (DS400; YAMATO scientific Co., Ltd, Japan) at 105°C for 5 hours to dry, and the water content was determined from the ratio of the weights of the samples before and after drying.

4.3. Results and discussion

4.3.1 Heating of wheat paste by laser

A wheat paste with 0.1% green dye was heated by the laser showed a scanned trace with a burnt region at the center (Fig. 2). The cross-section of the laser-scanned paste showed the dent which was possibility formed because of the evaporated water in the paste by heating at high temperature. The surface temperature profile of the wheat paste was measured using an IR camera which showed that the wheat paste was heated instantly at approximately 180°C (Fig. S1).

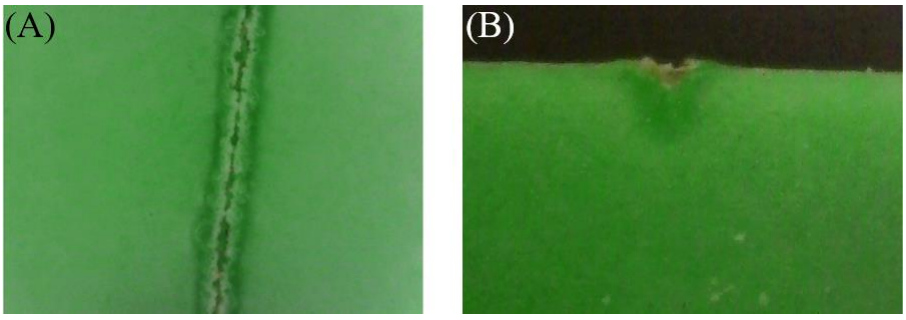

Fig. 2 Images of the wheat paste with added the green dye after laser heating. (A): surface; (B): cross-section.

4.3.2 Observation of optical and polarized microscopy and SEM

Starch granules are composed of amorphous and crystalline domains [11,12]. During gelatinization, the amorphous regions in the starch granules hydrate and swell, whereas the crystalline regions gradually melt with proceeding the hydration [13-15]. Fig. 3A-1 shows the cross-section of the wheat paste with 0.1% dye after laser heating observed by an optical microscope. It was observed that starch granules remained in the area away from the dent made

by the laser scan and changed to a melt. The observation by a polarized microscope in Fig. 3A-2 conformed that the granules kept crystalline structure and the melt contained no crystalline indicating that the crystal in granules was gelatinized[15,16]. The gelatinization area of starch granules was 0.13 mm from the surface of the dent and 0.25 mm from the deepest part of the dent.

SEM measurements were performed to observe the morphological changes of starch granules with laser heating. As shown in Fig. 3B, the structure of the starch granules in the gelatinization region collapsed and the granules fused with each other to form the gelatinized lumps. On the other hand, the starch structure of ungelatinized region was not changed.

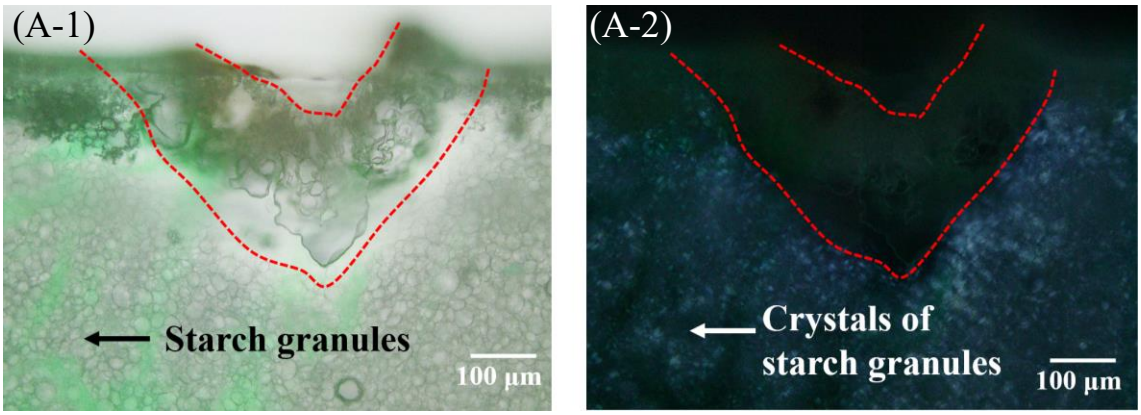

Fig. 3A Images of optical and polarized microscope of cross-section of the wheat paste after laser heating.
(A-1): optical microscope; (A-2): polarized microscope.

(B)

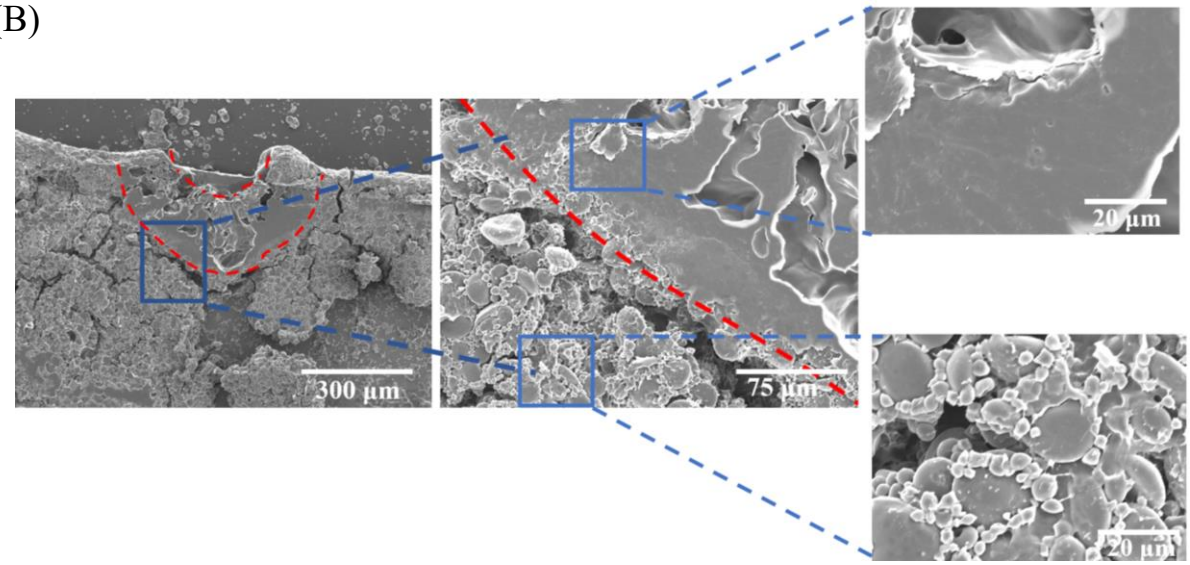

Fig. 3B Images of electric scanning microscopy of cross-section of the wheat paste after laser heating.

4.3.3 MRI

Measurements of water ^{1}H T_2 provide information about starch-water interactions and the mobility of polysaccharide chains through chemical exchange between water protons and the exchangeable protons of polysaccharides [17], which are largely affected by the gelatinization [18]. To visualize the special distribution of gelatinization state in the laser-heated wheat paste, T_2 weighted images were measured by MRI. The brightness of the image is proportional to the signal intensity at the echo time of 9.4 ms. As shown in Fig. 4A, the unheated wheat paste was darker than the reference. This suggests that the starch chains dispersed out from granules, which have a stiff conformation like being in a crystalline, decreased the observed water ^{1}H T_2 through the chemical exchange [19-21]. It is also possible that the difference in the magnetic

susceptibility of the water and wheat flour caused the inhomogeneous bulk magnetic susceptibility of the paste [22]. On the other hand, the heated region was brighter than the non-gelatinized region after gelatinization. This result is attributed to an increase in the mobility of starch chains due to gelatinization to make the observed ^{1}H T_2 longer than that in the non-gelatinized region with the stiff starch chain [20,21].

It should be noted that the non-gelatinized region was darker than that of the unheated sample. This indicating that the water content in the non-gelatinized region decreased when the laser heating caused the gelatinization in the central area. A possible explanation is that water demand of gelatinized starch increased to complete the hydration at the gelatinized state by absorbing water from non-gelatinized region, resulting in water migration (Fig 4B).

To confirm the hypothesis, a one side of model paste sheet with a thickness of 1 mm was heated at 200°C with keeping another side at 0°C by covering a cold plate and the water content of the heated and unheated sides were measured. The heated side was completely gelatinized, and the water content was about 57%, and another side remained non-gelatinized, and the water content was 43%, respectively. These results supported the hypothesis for the water migration in millimeter order seen in the MRI result.

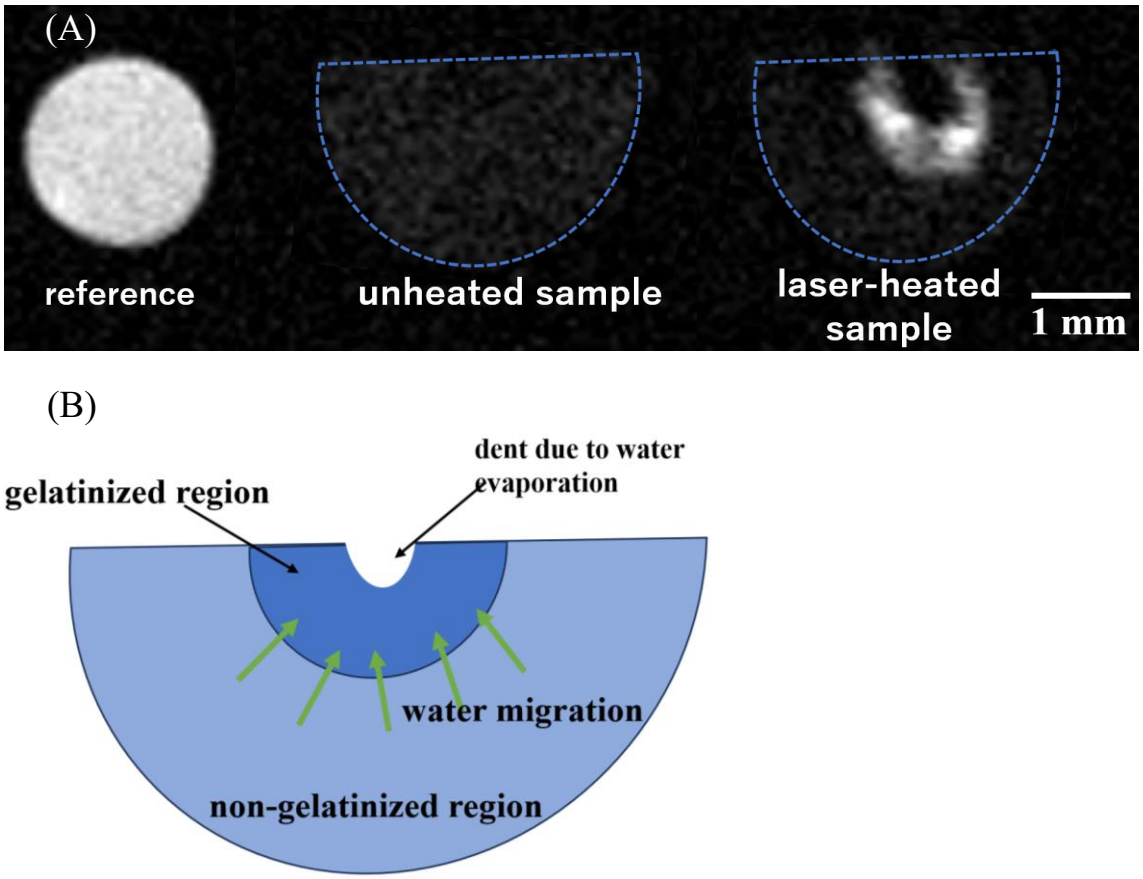

Fig. 4. T2 weighted image (TE = 9.4 ms) of cross-section of the wheat paste after laser heating.
(A): T2 weighted image of unheated wheat paste and laser heated wheat paste. The image in the circle is a reference of 40 % (*w/w*) sucrose solution. (B): schematic picture of mechanism of wheat paste gelatinization by laser heating.

The water uptake rate of the gelatinized region from the non-gelatinized region was also qualitatively investigated by MRI. Two lasers were scanned at 2 mm intervals on the wheat paste with added dye (0.1% w/w). Two or 10 seconds later, the lasers were scanned at the center of the interval between the first two scanned lasers (Fig. 5A), and T_2 weighted images were measured by MRI. The paste scanned by the laser after 2 s and that scanned after the 10 s are shown in Fig. 5B-1 and Fig. 5B-2, respectively. In Fig. 5B-1, three scanned line showed almost

same size for gelatinization region. In Fig. 5B-2, on the other hand, the gelatinized region for outer two lines became larger than those in Fig. 5B-1 and the center gelatinized region became smaller. These results indicate that the region heated by laser started absorbing water from the region around to swell and decrease water content in the surrounding in 10 s, which repressed the gelatinization by the third laser scan at the central region [23]. This finding demonstrates the possibility of unexpected difficulty by the decrease of water content.

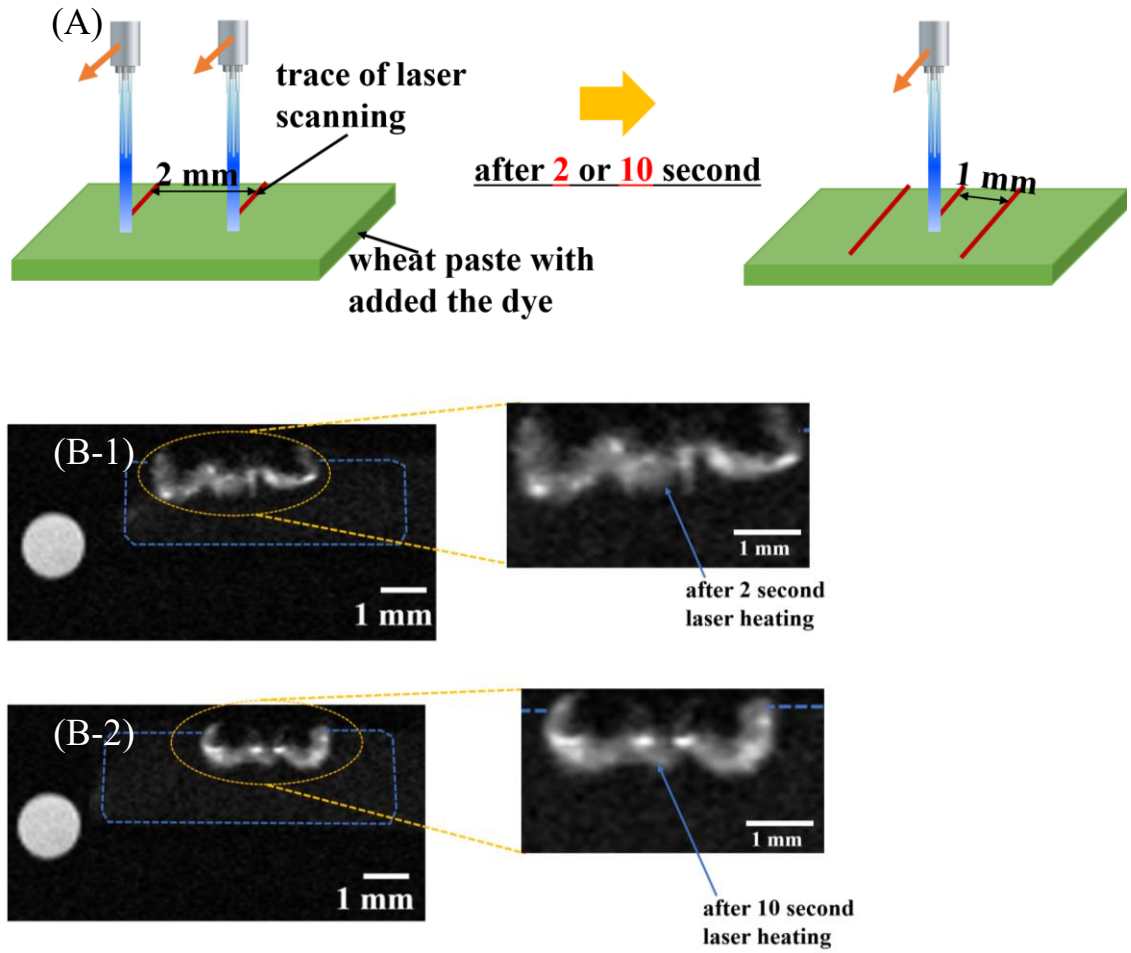

Fig. 5. Experimental setup and T2 weighted image (TE = 9.4 ms) of cross-section of the wheat paste after laser heating.
(A): Experimental setup; (B-1): after 2 second laser heating; (B-2): after 10 second laser heating.

4.4. Conclusions

The gelatinization of wheat starch paste by a laser irradiation and subsequent water migration in the paste during gelatinization was elucidated. Observation of the cross-section by a polarized microscope showed the melting of starch granule crystals in the laser heated region and SEM observation indicated the collapse of starch granules to give the gelatinized lumps engulfing the water. The MRI measurements suggested that the gelatinized region by the laser heating absorbed water from the non-gelatinized region to decrease the water content and repress the gelatinization in the surrounding area. This phenomenon is an important consideration for laser cooking processes, such as 3D food printing, which suggests a possibility of inhomogeneous water distribution would occur in printed food products due to the water migration of food ink during laser cooking. It is also suggested a possibility of controlling the gelatinization range and water content by changing laser heating conditions. Conclusively, our study is expected to provide useful knowledge for the application of laser heating in the food industry, such as 3D food printing.

4.5. Reference

1. Blutinger JD, Cooper CC, Karthik S, Tsai A, Samarelli N, Storvick E, Seymour G, Liu E, Meijers Y, Lipson H. The future of software-controlled cooking. NPJ Sci Food. 2023; 7 (1). 6. doi: https://doi.org/10.1038/s41538-023-00182-6.
2. Blutinger JD, Meijers Y, Lipson H. Selective laser broiling of Atlantic salmon. Food Res Int 2019; 120. 196-208. doi: https://doi.org/10.1016/j.foodres.2019.02.043.
3. Blutinger JD, Tsai A, Storvick E, Seymour G, Liu E, Samarelli N, Karthik S, Meijers Y, Lipson H. Precision cooking for printed foods via multiwavelength lasers. NPJ Sci Food. 2021; 5 (1). 24. doi: https://doi.org/10.1038/s41538-021-00107-1.
4. Shabir I, Khan S, Dar AH, Dash KK, Shams R, Altaf A, Singh A, Fayaz U, Majeed T, Khan SA, Pandey VK. Laser beam technology interventions in processing, packaging, and quality evaluation of foods. Measurement: Food 2022; 8. 100062-100073. doi: https://doi.org/10.1016/j.meafoo.2022.100062.
5. Dong H, Wang P, Yang Z, Xu X. 3D printing based on meat materials: Challenges and opportunities. Curr Res Food Sci 2023; 6. 100423-100433. doi: https://doi.org/10.1016/j.crfs.2022.100423.
6. Jonkers N. Dommelen, JAW, Geers MGD. Selective Laser Sintered food: A unit cell approach to design mechanical properties. J Food Eng. 2022; 335. 111183-111192. doi: https://doi.org/10.1016/j.jfoodeng.2022.111183.
7. Jonkers N. Dommelen, JAW, Geers MGD. An anisotropic elasto-viscoplastic-damage model for Selective Laser Sintered food. Eng Frac Mech. 2022; 266. 108368-108387. doi: https://doi.org/10.1016/j.engfracmech.2022.108368.
8. Shahbazi M, Jäger H, Ettelaie R. Kinetic evaluation of the starch molecular behavior under extrusion-based or laser powder bed fusion 3D printing systems: A systematic structural and biological comparison. Addit Manuf. 2022; 57. 102934-102948. doi: https://doi.org/10.1016/j.addma.2022.102934.
9. Blutinger JD, Meijers Y, Chen PY, Zheng C, Grinspun E, Lipson H. Characterization of dough baked via blue laser. J Food Eng. 2018; 232, 56-64. doi: https://doi.org/10.1016/j.jfoodeng.2018.03.022.
10. Blutinger JD, Meijers Y, Chen PY, Zheng C, Grinspun E, Lipson H. Characterization of CO2 laser browning of dough. IFSET. 2019; 52, 145-157. doi: https://doi.org/10.1016/j.ifset.2018.11.013.
11. Rodriguez GME, Hernandez LMA, Delgado JM, Ramirez GCF, Ramirez CM, Millan MBM, Londoño RSM. Crystalline structures of the main components of starch. Curr Opin Food Sci. 2021; 37, 107-111. doi: https://doi.org/10.1016/j.cofs.2020.10.002.
12 Zhu F. Relationships between amylopectin internal molecular structure and physicochemical properties of starch. Trends Food Sci Technol. 2018; 78, 234-242. doi:

https://doi.org/10.1016/j.tifs.2018.05.024.
13. Chakraborty INP, Mal SS, Paul UC, Rahman MH, Mazumder N. An Insight into the Gelatinization Properties Influencing the Modified Starches Used in Food Industry: A review. Food Bioproc Tech. 2022; 15 (6), 1195-1223. doi: 10.1007/s11947-022-02761-z.
14. Palanisamy A, Deslandes F, Ramaioli M, Menut P, Plana FA, Flick D. Kinetic modelling of individual starch granules swelling. Food Struct. 2020; 26, 100150-100161. doi: https://doi.org/10.1016/j.foostr.2020.100150.
15. Tao J, Huang J, Yu L, Li Z, Liu H, Yuan B, Zeng D. A new methodology combining microscopy observation with Artificial Neural Networks for the study of starch gelatinization. Food Hydrocoll. 2018; 74, 151-158. doi: https://doi.org/10.1016/j.foodhyd.2017.07.037.
16. Chen X, Du X, Chen P, Guo L, Xu Y, Zhou X. Morphologies and gelatinization behaviours of high-amylose maize starches during heat treatment. Carbohydr Polym. 2017; 157, 637-642. doi: 10.1016/j.carbpol.2016.10.024.
17. Lewis GP, Derbyshire W, Ablett S, Lillford PJ, Norton IT. Investigations of the n.m.r. relaxation of aqueous gels of the carrageenan family and of the effect of ionic content and character. Carbohydr Res. 1987; 160(15), 397-410; doi: https://doi.org/10.1016/0008-6215(87)80326-9.
18. Donmez D, Pinho L, Patel B, Desam P, Campanella OH. Characterization of starch–water interactions and their effects on two key functional properties: starch gelatinization and retrogradation. Curr Opin Food Sci. 2021; 39, 103-109. doi: https://doi.org/10.1016/j.cofs.2020.12.018.
19. Zhang Q, Matsukawa S, Watanabe T. Theoretical analysis of water 1H T2 based on chemical exchange and polysaccharide mobility during gelation. Food Hydrocoll. 2004; 18 (3), 441-449. doi: https://doi.org/10.1016/j.foodhyd.2003.08.002.
20. Tananuwong K, Reid D. DSC and NMR relaxation studies of starch water interactions during gelatinization. Carbohydr Polym. 2004; 58 (3), 345-358. doi: https://doi.org/10.1016/j.carbpol.2004.08.003.
21. Tang HR, Brun A, Hills B. A proton NMR relaxation study of the gelatinisation and acid hydrolysis of native potato starch. Carbohydr Polym. 2001; 46, 7-18. doi: S0144-8617(00)00265-4.
22. Chu, KC, Xu Y, Balschi JA, JR CSS. Bulk magnetic susceptibility shifts in NMR studies of compartmentalized samples: use of paramagnetic reagents. Magnetic Resonance in Medicine 1990; 13 (2), 239-262. doi: 10.1002/mrm.1910130207.
23. Altay F, Gunasekaran S. Influence of Drying Temperature, Water Content, and Heating Rate on Gelatinization of Corn Starches. J Agric Food Chem. 2006; 54, 4235−4245. doi: 10.1021/jf0527089.

5. General Summary

The water uptake behavior of food powders and the gelatinization behavior of starch by localized heating using laser irradiation were elucidated in order to realize the industrial application of stereolithography 3D food printing. These physical properties are important for the development of food ink preparation techniques in the 3D food printing. The remarkable results of this theses are summarized below:

1. The potato powder exhibited higher water uptake than the soybean powder, a result which was attributed to the different powder compositions. Potato and soybean powders exhibited different wetting, swelling and dispersion behaviors in water. MRI experiments also demonstrated the difference in water uptake between the powders, and indicated the formation of air bubbles, which could hinder water uptake. Numerical simulations based on a gravity-corrected Washburn-model were further performed to elucidate the mechanism of water uptake. The simulations and experiments were in good agreement. We demonstrated that powder swelling, and a dissolution-driven viscosity increases opposed water uptake and produced an eventual plateau. Our results suggest that the model used in our simulation can explain the effects of powder swelling and viscosity changes on water uptake.

2. The localized heating by laser irradiation caused the gelatinization of the paste in a millimeter order width which caused a subsequent water migration from the ungelatinized region by the water demand associated with the gelatinization. Polarized microscopy, scanning electron

microscope (SEM) observation and magnetic resonance imaging (MRI) have been carried out for the elucidation. The cross-section observation by a polarized microscope showed the melting of starch granule crystals in the laser heated region, and SEM observation indicated the collapse of starch granules to give the gelatinized lumps engulfing the water. MRI measurements gave the distribution of water content in the laser heated paste suggesting the water migration from the ungelatinized region where the gelatinization by the following laser heating was restrained because of the low water content.

Conclusively, these results provide useful information on developing the technology for improving the water uptake of food powders for food inks and laser cooking techniques, enabling potential applications in the food processing industry including 3D food printing.

Acknowledgment

I heartily thank my supervisor, Prof. Matsukawa, for his dedication and supervision. I deeply appreciate all his support and encouragement during my Ph.D. program in the last three years. This work could not be brought towards a completion his supervision. I would also like to thank the committee members, Prof. Osako, Prof. Takahashi, Prof. Fukuoka, and Prof. Ivan for taking the time and effort to give thoughtful advice.

I am grateful to my fellow laboratory of Food Bussei members. Special thanks to Dr. Xi Yang for kindly helping me through revising our publications and my doctoral thesis.

Finally, my biggest thanks to my family who have been encouraging and supporting me.

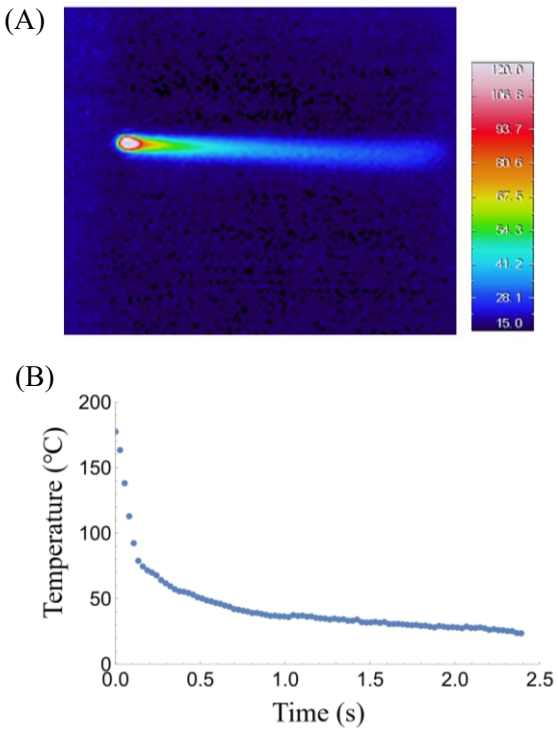

Fig. S1 Temperature profile of the wheat paste with added the dye during laser heating.
(A): IR image of the wheat paste; (B): Changes in temperature over time during laser heating. A line was drawn through the center of the temperature distribution in the IR image, and the temperature profile was calculated from the temperatures indicated by the pixels on the line and laser scanning time.